ENGINEERING

Exploiting radiative cooling for uninterrupted 24-hour water harvesting from the atmosphere

Iwan Haechler, Hyunchul Park, Gabriel Schnoering, Tobias Gulich, Mathieu Rohner, Abinash Tripathy, Athanasios Milionis, Thomas M. Schutzius*†, Dimos Poulikakos*

Copyright © 2021 The Authors, some rights reserved; exclusive licensee American Association for the Advancement of Science. No claim to original U.S. Government Works. Distributed under a Creative Commons Attribution NonCommercial License 4.0 (CC BY-NC).

Atmospheric water vapor is ubiquitous and represents a promising alternative to address global clean water scarcity. Sustainably harvesting this resource requires energy neutrality, continuous production, and facility of use. However, fully passive and uninterrupted 24-hour atmospheric water harvesting remains a challenge. Here, we demonstrate a rationally designed system that synergistically combines radiative shielding and cooling—dissipating the latent heat of condensation radiatively to outer space—with a fully passive superhydrophobic condensate harvester, working with a coalescence-induced water removal mechanism. A rationally designed shield, accounting for the atmospheric radiative heat, facilitates daytime atmospheric water harvesting under solar irradiation at realistic levels of relative humidity. The remarkable cooling power enhancement enables dew mass fluxes up to 50 g m^{-2} $hour^{-1}$, close to the ultimate capabilities of such systems. Our results demonstrate that the yield of related technologies can be at least doubled, while cooling and collection remain passive, thereby substantially advancing the state of the art.

INTRODUCTION

Two-thirds of humanity live under conditions where the net freshwater withdrawal is more than twice the natural water availability for at least 1 month per year, and half a billion people suffer from this water stress throughout the entire year (*1*, *2*). While currently there is enough fresh water on earth to support consumption, it is not available in a way where supply meets demand (*3*–*5*). Growing global challenges, such as climate change, human population growth, and their combination, pose additional detrimental threats to global water resources (*6*). Atmospheric water vapor represents an alternative source for potable water due to its vast total amount and universal accessibility. In fact, the bulk of water in the atmosphere in wet and dry regions could provide an additional ~15% of fresh water to the existing sources (*7*). This amount is equivalent to nearly three times the yearly global water consumption (*6*). Harnessing this resource sustainably, however, has proven difficult. Because of the large enthalpy of condensation of water, active methods require substantial energy resources or rely on refrigerants (*8*), which contribute further to global warming or ozone depletion. Passive methods usually have low yields (*9*–*11*), driving recent research on improving the yield of such systems (*12*, *13*).

Passive water harvesting systems can be classified as either sorbent-based [daytime operation, low relative humidity (RH)] or radiative cooling–based dew harvesting (nighttime operation, high RH). Recently, sorbent-based approaches have been extensively studied with newly developed materials (*14*–*16*). In a sorbent-based water harvesting system, desiccants such as metal-organic frameworks, silica gels, zeolites, deliquescent salts, or activated alumina are used to adsorb water vapor in an open chamber, simulating the atmospheric environment (*17*–*19*). Once the desiccant is saturated, the system is closed and naturally heated with sunlight, causing it to release the water as vapor. Last, the vapor condenses on the enclosure walls and can be collected. Sorbent-based systems have shown that water vapor can be harvested at a very low RH (as low as 15%) (*12*). Although the energy for vaporization comes from the sun, the cyclic nature of these systems requires input of active work to switch between cycles. The dependency on sunlight for desorbing the water vapor implies that water can only be harvested during daytime.

A conventional radiative cooling foil that is used for dew harvesting emits thermal radiation in the wavelength range where the atmosphere is mostly transparent (8 to 13 μm) and can therefore directly emit heat radiatively to space. This effect cools the foil below the dew point temperature of air, causing water to condense upon it, which is termed "dewing" (*20*). Fortunately, most regions affected by high water scarcity have a natural advantage of abundant sunshine and hence a clear sky, which are optimal conditions for radiative cooling (*21*). A commonly used dew harvesting foil is from OPUR (Organisation Pour l'Utilisation de la Rosée), which consists of TiO_2 and $BaSO_4$ microspheres embedded in a polyethylene film. With this foil, nighttime dew harvesting has been demonstrated with yields of up to ~40 g m^{-2} $hour^{-1}$ at RH > 60% (*22*–*29*). Given the fundamental theoretical limit of 59 g m^{-2} $hour^{-1}$ at 100% RH (*30*)—obtained through a theoretical analysis by assuming no sunlight illumination, an RH of 100%, and neglecting any potential convective heat gains—these water yields are impressive, because the conditions during the experiments were at a lower RH and without actively pumped, convective air flow. However, the drawback of this foil is that it only works during nighttime because it absorbs near-infrared (IR) sunlight.

Recently, through proper spectral engineering, radiative cooling of surfaces below ambient temperature could be achieved even during daytime by limiting sunlight absorption while maximizing the emissive properties in the IR range (>2.5 μm) (*31*–*34*). On the basis of this principle, condensation enhancement in a solar water purification system has been shown, wherein supersaturated steam (i.e., steam at a temperature above ambient) is actively pumped to the condenser (*35*). While a lot of research has focused on optimizing the emissive properties and facility of fabrication of daytime

Laboratory of Thermodynamics in Emerging Technologies, Department of Mechanical and Process Engineering, ETH Zurich, Sonneggstrasse 3, CH-8092 Zurich, Switzerland.
*Corresponding author. Email: dpoulikakos@ethz.ch (D.P.); thomschu@ethz.ch (T.M.S.)
†Present address: Laboratory for Multiphase Thermofluidics and Surface Nanoengineering, ETH Zurich, Sonneggstrasse 3, ML J 27.2, CH-8092 Zürich, Switzerland.

cooling materials (*36*, *37*), little attention has been paid to the important aspect of effectively controlling the inherent interaction of the surrounding radiative environment and such selective emitter surfaces (*38*–*40*). Moreover, for condensation applications, due to the intrinsic wetting properties of existing systems, the condensate remains on the surface and has to be actively removed. For example, up to 51% of the dew remains on the foil of OPUR (*26*), which has to be collected by scraping off the surface actively in the early morning hours (*41*). Hence, none of the above existing approaches (sorption-based water harvesting devices or radiative cooling–based dew harvesting foils) are designed to be operating continuously for 24 hours or without any external intervention and are therefore not fully passive.

Here, we demonstrate continuous, 24-hour water collection driven by radiative cooling under atmospheric conditions, in a fully passive manner, alleviating serious drawbacks of the state of the art and making a major step toward continuous and passive, fully energy-neutral atmospheric water harvesting becoming a viable real-life process. Our approach decouples the design and optimization of the performance of the cooling and dewing functions, and focuses on two important but overlooked aspects, namely, diffuse radiative heat from the surrounding environment and truly passive efficient removal of condensate. Unlike in solar water purification where the system can operate at ambient temperature (because the delivered humid air is supersaturated), in the case of dew harvesting, an atmospheric water harvesting system first needs to cool itself to the dew point temperature. Once this temperature is reached, the cooling power that is still available can be used for the latent heat uptake of the condensate. We optimized our system by using a rational balance of subambient cooling while sustaining a high cooling power (for the latent heat uptake) even once the desired temperature is reached. To achieve this, we account for not only the spectral (*35*) but also the spatial dependence of the atmospheric radiative heat gains (*36*, *38*–*40*, *42*). This important interplay of subambient cooling and conservation of high cooling power can substantially boost the dew harvesting potential of atmospheric water harvesting systems. Consequently, daytime dew harvesting is possible without requiring forced flow or supersaturated, humidified air used earlier (*35*). The system emits thermal radiation to cold space through the 8- to 13-μm wavelength transparency window of the atmosphere and fully accounts for all heat transfer modes, including the surrounding radiative environment. On the basis of a complete analysis of the involved heat fluxes and experimental constraints, a geometrically optimized radiation shield directs thermal radiation toward the normal incidence, i.e., where the atmospheric transmittance is highest. Simultaneously, the radiation shield guards the cooling surface from atmospheric radiation coming from the horizon. The combination of these two mechanisms, i.e., accounting for both incoming and outgoing thermal radiation, is the essential factor for the success of our system, which reaches more than double the yield of existing systems. We exploited this radiative cooling working collaboratively with a special superhydrophobic dropwise condensation and water collection mechanism (jumping droplet coalescence) in a decoupled, not mutually hindering manner, which enables optimization of both these critical functionalities individually. For success of atmospheric water harvesting systems, complete passiveness is highly desirable. The added functionality of the superhydrophobic collection surface is to inhibit filmwise and instead enhance dropwise condensation, leading to rapid and facile water self-removal fully passively, allowing our system to realize atmospheric water collection without requiring any work or user intervention.

RESULTS

System design and working principle

To achieve continuous, efficient, and completely passive atmospheric water harvesting, we depart from previous approaches and separate the radiative cooling and water collection surfaces to eliminate inherent, mutually destructive, interferences of their functionalities and allow individual tailoring of each, as shown in Fig. 1A. Akin to existing daytime cooling materials, our surface exploits the atmospheric transparency window [wavelength (λ) = 8 to 13 μm] and emits thermal radiation to cold space, thereby cooling the selective emitter below ambient temperature. For other works that aim to achieve deep subambient temperatures, a spectrally selective design that only emits in the 8- to 13-μm range is favorable (*43*, *44*). However, for our application, where the goal is to maximize the cooling power that is freely available once the emitter cooled itself to the dew point temperature, a broader emission spectrum in the IR (>2.5 μm) is favorable (*35*, *39*, *44*–*47*). The selective emitter resides on a Styrofoam ring, with the radiation side facing upward (Fig. 1A). A transparent insulating film limits convective heat gains and dew formation on top of the selective emitter, which would hinder its function. A specially designed radiation shield accounts for the surrounding radiative environment of the emitter. The other (bottom) surface of the selective emitter is exposed to open air and is designed to promote dropwise condensation with a superhydrophobic coating, enabling condensate droplet removal through the existence of a droplet coalescence jumping mechanism (*48*–*52*). For dew to form, the selective emitter needs to cool the condensation surface below the dew point temperature T_{dew}, including removal of the latent heat of vaporization (Fig. 1A). To achieve this, the radiation side of our system consists of a selective emitter to radiatively dissipate its heat and reflect sunlight. Figure 1B shows the individual layers of the selective emitter with negligible thermal resistance. It consists of a radiative cooling coating (*53*) [a layer of polydimethylsilane (PDMS), 100 μm] on an IR-emissive glass substrate (500 μm thick), which is transparent to the visible light (*54*). The backside of this substrate is coated with a sunlight reflector (thin layer of silver, 140 nm). Two thin, conformal layers of chromium (0.5 and 1 nm, respectively) enhance the adhesion of the silver to the glass substrate and prevent oxidation on the other side. While this reflection layer is standard for radiative cooling (*35*, *36*, *55*), for large-area applications, this reflector can easily be replaced by other scalable reflection layers (*32*, *56*, *57*). Our spectrally selective emitter is—like previous approaches (*46*, *47*, *55*, *58*, *59*)—designed to deliver high emission in the sky transparency window and minimize interaction with the solar spectrum. Figure 1C shows a plot of the spectral emissivity (equal here to the absorptivity, $\varepsilon = \alpha$). The as-designed structure is strongly reflective, therefore poorly absorbing, in the solar range of the spectrum, i.e., visible and near-IR range for $\lambda \approx 0.25$ to 2.5 μm ($\overline{\varepsilon}_{0.25-2.5} = \overline{\alpha}_{0.25-2.5} \approx 0.04$). Outside this range, it shows a high average emissivity to maximize the thermally emitted power, especially in the range $\lambda \approx 8$ to 13 μm ($\overline{\varepsilon}_{8-13} = \overline{\alpha}_{8-13} \approx 0.93$), comparable to the spectral values of previous approaches (*31*, *60*). Hence, the values for $\overline{\varepsilon}_{0.25-2.5}$ and $\overline{\varepsilon}_{8-13}$ are close to the ones previously reported, and approximating the optimum ones ($\overline{\varepsilon}_{0.25-2.5} = 0$

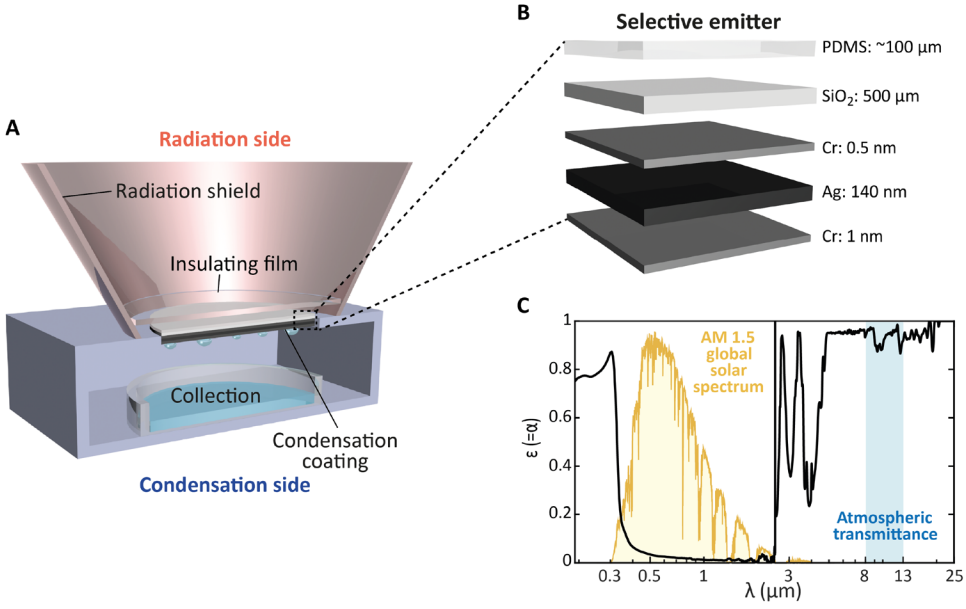


Fig. 1. Design of system. (**A**) Working principle with separated radiation and condensation side. The radiation shield—optimized by accounting for the surrounding radiative environment—allows one to improve substantially the dew harvesting potential of the system and can be applied for any selective emitter. (**B**) Structure of selective emitter. It consists of PDMS and silver, coated on a transparent glass substrate (chromium is used for oxidation protection and adhesion). (**C**) Measured spectral absorptivity/emissivity of the selective emitter. The average emissivity in the atmospheric transparency window is very high ($\bar{\varepsilon}_{8-13} \approx 0.93$), while the average absorptivity in the solar spectrum range is very low ($\bar{\alpha}_{0.25-2.5} \approx 0.04$).

and $\bar{\varepsilon}_{8-13} = 1$, respectively). In this work, the focus lies on enhancing the subcooling and thus water harvesting potential of our system by considering the surrounding radiative environment. We engineered a truncated cone-shaped structure from an aluminum sheet, covered with aluminized Mylar, and placed it around the selective emitter. The high reflectivity of the Mylar in the IR range directs thermal radiation from the selective emitter toward the normal incidence—where the atmospheric transmittance is highest—and strongly enhances the subcooling (to be discussed in detail later). Simultaneously, the structure protects and strongly truncates detrimental atmospheric radiation gains. Last, the insulating foil sits 2 cm above the selective emitter (see Fig. 1A) and consists of polyethylene, which is transparent in both the visible and IR range and allows radiation to pass through.

Heat flux analysis and atmospheric radiation shield design

Five heat fluxes contribute to the heat balance of the selective emitter: radiative cooling $\dot{Q}_{cool}$ (heat emission to space), radiative heat gains from the sun $\dot{Q}_{sun}$ and the atmosphere $\dot{Q}_{atm}$, plus convective heat gains $\dot{Q}_{conv}$ from the air surrounding the emitter and $\dot{Q}_{dew}$, which accounts for the latent heat gains during dew formation. The heat flux balance for a steady-state operation can be written as

$$\dot{Q}_{dew} = \dot{Q}_{cool} - (\dot{Q}_{sun} + \dot{Q}_{atm}) - \dot{Q}_{conv} \quad (1)$$

We calculate $\dot{Q}_{dew} = \dot{m}\, h_{fg}$, where $\dot{m}$ is the rate of condensate mass change and h_{fg} is the latent heat of condensation. Figure 2A shows the thermodynamic interaction of the selective emitter with the environment at a given RH, ambient temperature T_{amb}, and emitter temperature T_{sample}. In this experiment and all results of Fig. 2, the selective emitter rests on a Styrofoam block, which prevents condensation on its underside ($\dot{Q}_{dew} = 0$). This allows us to solely assess the cooling performance of the radiation side without the latent heat released from condensation. To boost $\dot{Q}_{dew}$ and the dew yield of our system, we maximize $\dot{Q}_{cool}$ through a near-unity emissivity of the selective emitter in the 8- to 13-μm range, similar to the state-of-the-art radiative cooling surfaces. Likewise, $\dot{Q}_{sun}$ is minimized due to the low absorptivity of the emitter surface in the solar range. The insulating film helps reduce the nonradiative heat coefficient h_c and thus $\dot{Q}_{conv}$, which is given by $\dot{Q}_{conv} = h_c(T_{amb} - T_{sample})$.

The rational design of the radiation shield accounts for the radiative environment of the selective emitter, i.e., the angular dependence of the atmospheric emissivity $\varepsilon_{atm}(\Theta, \lambda)$ (*45*), to further minimize $\dot{Q}_{atm}$. Within the sky transparency window, i.e., where the selective emitter is designed to absorb and emit most of the radiation, the atmospheric emissivity is highest at the horizon ($\Theta \to 90°$) and lowest toward $\Theta = 0°$, as depicted in Fig. 2A (*42*). First, the radiation shield protects the emitter from atmospheric radiation $\dot{Q}_{atm}$ coming from high Θ. Second, $\dot{Q}_{cool}$ is maximized by directing all the emitted thermal radiation of the selective emitter (0° to 180°) toward $\Theta = 0°$ (*39*), where the atmospheric transmittance is highest. We determined the optimal half-opening angle β of the radiation shield (see Fig. 2A) to optimize the nonlinear interplay of $\dot{Q}_{atm}$ and $\dot{Q}_{cool}$ by using a geometrical raytracing model (*61*), accounting for experimental constraints such as the emitter spectral emissivity $\varepsilon_{sample}(\lambda)$, shield height H, base radius r, and a range of values of Mylar reflectivity R (see the Supplementary Materials and fig. S1). Our analysis leads to a choice of $\beta \approx 30°$. With this given β, one can define a shielding angle φ, which is geometrically related by $\tan\varphi = H/(2r + H\tan\beta)$, as shown in Fig. 2A. The radiation shield leads to a suppression of atmospheric radiative heat gains coming from $\Theta > (90° - \varphi)$. In addition, as the shield is reflective in the solar range, $\dot{Q}_{sun} = 0\ W\ m^{-2}$ whenever the sun zenith angle $\Theta > (90° - \varphi)$, thus further boosting the performance of the selective emitter (*62*).

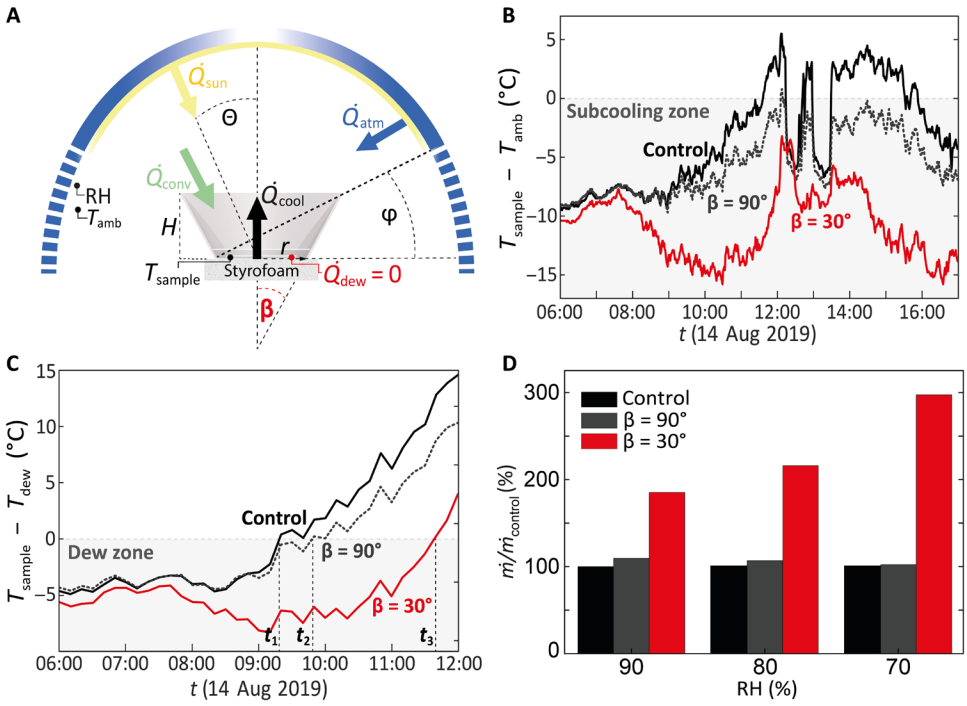


Fig. 2. Subcooling and dew harvesting potential enhancement through the radiation shield. (**A**) Thermodynamic analysis of the radiation shield and involved heat fluxes. Styrofoam blocks condensation side, consequently $\dot{Q}_{dew} = 0$. The angular dependence of atmospheric emissivity is represented in blue. (**B**) Subcooling performance of OPUR, selective emitter with (β = 30°) and without (β = 90°) radiation shield. (**C**) Theoretical dew harvesting potential. The selective emitter, working collaboratively with the radiation shield, extends the harvesting window by more than 2 hours (t_1 to t_3) and to conditions with RH < 50% and 808 W m^{-2} solar irradiation (10-min intervals). (**D**) Improvement of the state of the art. The selective emitter, collaboratively working with the radiation shield, outperforms existing dew harvesting technologies by a factor 2 to 3 depending on RH.

While we optimized the radiation shield based on the optical properties of our selective emitter (see Fig. 1C), this approach can be applied to any selective emitter to further boost the cooling performance. Accounting for the spatial dependence of the atmospheric radiation not only boosts the performance of an emitter with a broad emission spectrum in the IR. Our approach would also enhance the performance of a perfectly selective emitter that only emits in the 8- to 13-μm range, as the radiation shield substantially reduces atmospheric radiative heat gains within this window (see fig. S2).

We experimentally assessed the effect of the radiation shield on the subcooling performance and recorded the temperatures of the ambient, a bare selective emitter (β = 90°), a selective emitter with radiation shield (β = 30°), and a control sample (OPUR-foil, β = 90°) on the roof of a building at ETH Zurich (latitude 47.377747, longitude 8.547607) on 13 to 14 August 2019 for 24 hours (further experiments to test the effect of the radiation shield on the subcooling performance can be found in the Supplementary Materials and figs. S3 and S4). Figure 2B shows a plot of the subcooling from 06:00 on 14 August 2019 until the end of the run at 17:00 (see the Supplementary Materials and fig. S5 for the full experimental data). While the sun is absent at night ($\dot{Q}_{sun}$ = 0 W m^{-2}), the atmosphere still emits. Hence, even before dawn (06:20), the radiation shield helps minimize $\dot{Q}_{atm}$, resulting in a higher subcooling. After sunrise, the selective emitter with radiation shield markedly outperforms the other two samples, as theoretically predicted. The three distinct peaks around 12:30 and 13:00 and 14:00 arise due to clouds, reducing the sky transparency and deteriorating the cooling ability.

To quantify the implications of this result for dew harvesting under direct sun exposure, we computed T_{dew} based on the measured RH and T_{amb}. Figure 2C shows how the selective emitter allows to extend the time period for dew harvesting (i.e., $T_{sample} \leq T_{dew}$) into the day (for a more detailed quantitative analysis, see the Supplementary Materials and fig. S6). While the control (OPUR) is theoretically able to harvest dew until 09:20 (t_1), our selective emitter extends this window until 09:50 (t_2). What is more, at t_1, while for the control $T_{sample} = T_{dew}$, the temperature of the selective emitter with radiation shield at t_1 stays >5°C below T_{dew}, showing strong potential to still harvest dew, whereas the control as well as the bare selective emitter fail. Through the synergistic effect of the radiation shield and the selective emitter, the dewing period is significantly extended [by almost 2.5 hours until 11:40 (t_3)] compared to the bare selective emitter and the control. Even under the severe conditions at t_3 [summer in Zurich, RH (t_3) = 47%, T_{amb} (t_3) = 19°C, 808 W m^{-2} solar irradiation], the subcooling is such that the system can harvest dew. As $\dot{Q}_{dew}$ = 0 W m^{-2} during the entire experiment, any available $\dot{Q}_{cool}$ is converted into a higher subcooling ($\dot{Q}_{conv}$). However, for dew harvesting, as soon as T_{sample} reaches T_{dew}, any cooling power that is still freely available is used to take up the latent heat of condensation, h_{fg}, and to collect dew. Hence, we calculated the instantaneous subcooling below T_{dew} for all samples and determined a theoretically achievable $\dot{m}$, corresponding to the case where all subcooling below T_{dew} is used for $\dot{Q}_{dew}$ (i.e., no cooling of noncondensable gases). Figure 2D presents the ratio of $\dot{m}$ for our selective emitter with (β = 30°) and without (β = 90°) radiation shield, assuming a constant RH of 70, 80, and 90% and normalized to the rate of

condensate mass change for OPUR, $\dot{m}_{control}$. While the selective emitter allows us to decouple the radiation and condensation side and optimize both functions individually, functioning alone, it only leads to an improvement of a few percent over the state of the art, highlighting the strength of OPUR foil. However, when the selective emitter works collaboratively with the optimized radiation shield, the yield of the state of the art can be substantially outdone. While the selective emitter alone extends the dewing window from night into the day and leads to an improvement in the subcooling, the radiation shield boosts the dew harvesting potential. At RH = 90%, our system (β = 30°) produces 85% more water as OPUR and 75% more than the bare selective emitter. At lower RH, the advantage becomes even more striking, resulting in a nearly three times higher $\dot{m}$ at 70% RH compared to OPUR and the selective emitter without radiation shield.

Dew harvesting experiments

After the rational design of the radiation side discussed above, we next target dew harvesting during daytime, experimentally. To this end, an environmental chamber, on top of which our system sits, enables us to control the RH (using supersaturated salt-water solutions) of the atmosphere exposed to the water harvesting surface, as schematically depicted in Fig. 1A (for full details, see the Supplementary Materials and fig. S7). Because of the low thermal mass of the chamber, the air temperature inside is convectively equilibrated (due to wind) with the ambient temperature. We covered the chamber with aluminized Mylar to prevent heating through the greenhouse effect. Hence, the air temperature inside the chamber is very close to the ambient temperature (see fig. S8). The first experiment started on 26 July 2019 at 09:24, at RH > 90%, to qualitatively observe dew harvesting in this configuration by lifting the emitter every hour to image its condenser side. As Fig. 3A shows, dew rapidly accumulates, clear evidence that our system can use its cooling power to dissipate the latent heat of condensation of water, harvesting dew even under high solar irradiation ($I_{max} \approx 870$ W m^{-2}). Because of the higher subcooling required to reach T_{dew} at a lower RH, more of the emitter cooling power is consumed to counteract convective and radiative heat gains ($\dot{Q}_{conv}$ and $\dot{Q}_{atm}$) at such conditions. Consequently, $\dot{Q}_{dew}$ is reduced and dew harvesting becomes more restricted under lower RH conditions. To evaluate the effect of this, we set the RH at 95, 90, 75, and 65% and imaged the condensation side 90 min after the start of each experiment. Figure 3B demonstrates that our system is practically capable of harvesting dew at RH as low as 65%. This capability is consistent with our previous prediction; as previously outlined in Fig. 2D, the bare selective emitter alone without radiation shield would fail to harvest dew at this lower RH, highlighting the strength of the shield and to account for the surrounding radiative environment.

To quantify the water harvesting performance, we perform further experiments and measure the dew formation on the condensation side with a balance. The dew mass flux

$$\dot{\rho}_A = \frac{\dot{m}}{A} \tag{2}$$

where A is the condenser side area, is shown in Fig. 3C with the solar irradiation for a 24-hour run on 26 to 27 August 2019 with RH > 90%. $\dot{\rho}_A$ is almost continuously positive, showing the impressive performance of the continuous water harvesting system. Additional experiments seen in Fig. 3D underpin its continuity and broad operational capability, where we show the mean solar irradiation $\bar{I} = \frac{1}{\Delta t}\int I\,dt$ and corresponding mean dew mass flux $\bar{\rho}_A = \frac{1}{\Delta t}\int \dot{\rho}_A\,dt$ of all experimental runs, where $\Delta t = t_{end} - t_{start}$. For a value of $\bar{I} \approx 200$ W m^{-2}, and at a mean RH of 96%, our system achieves $\bar{\rho}_A > 52$ g m^{-2}hour^{-1} over a period of nearly 3 hours (30 August 2019; see table S1). While this value is achieved under controlled conditions, this result is very close to the theoretical perfect blackbody limit of 59 g m^{-2} hour^{-1} (*30*). The results show that by accounting for the radiative environment of the emitter, our system can maximize its cooling power available for condensation and even approach the theoretical limit. The $\bar{\rho}_A$ of our system is especially impressive given that the theoretical limit is obtained assuming no sunlight illumination, an RH of 100%, and neglecting any potential convective heat gains ($\dot{Q}_{conv} = 0$ W m^{-2}) conditions, markedly less challenging than the conditions under which our experiments were performed. Note that for these experiments, dew still remains on the condenser surface. Its fully passive removal is achieved with the subsequent incorporation of a superhydrophobic coating on the collection surface.

Passive self-removal of harvested dew

An important aspect of our, and any, atmospheric water harvesting system is the ability to remove and collect dew from the condenser surface without expenditure of additional energy input. Previous related systems require an active switching (usually by an operator) to the desorption cycle (*17*–*19*, *63*) or, for the case of dew-harvesting foils, dew is manually scraped off the surface, thus also requiring additional energy and active intervention (*26*, *41*). Therefore, it is important to reduce the critical size of water droplets falling from the dewing surface via surface engineering, because water droplets attached to the surface hinder an efficient heat transfer and suppress dew formation. A superhydrophobic condenser surface design, such that a gravity-independent jumping mechanism of the droplets emerges (*48*, *64*) and dew is passively removed, allows to operate fully autonomously and passively. When small droplets (~10 to 100 μm) coalesce on these nanostructured superhydrophobic surfaces, the reduction in surface energy leads to a coalescence-induced jumping of the droplets without any additional energy requirement (*48*). While the superhydrophobicity has an effect on $\dot{\rho}_A$, the system gains the functionality of complete passivity, a crucial factor for the real-world feasibility of atmospheric water harvesting systems. The detached water can then simply be collected and stored in a small reservoir underneath the surface, as illustrated in Fig. 1A.

The condenser surface with favorable wettability for droplet detachment is a thin, hierarchically micro-/nanostructured superhydrophobic coating that can be spray-coated onto the bottom side of our selective emitter (*64*), as illustrated in Fig. 4A. There is a range of superhydrophobic coatings promoting dropwise condensation (*49*–*52*). For reasons of heat transfer efficiency and ease of application, we opted to use a state-of-the-art thermally conductive, superhydrophobic carbon nanofiber (CNF), polymer composite (*64*). We used a dispersion of CNF and polytetrafluoroethylene (PTFE), featuring minimal thermal resistance and outstanding heat transfer performance compared to uncoated control metallic surfaces (*64*). The thermal conductivity of the CNF coating is estimated to be 0.30 to 5.37 W m^{-1} K^{-1} (*64*). As this sprayable coating is fabricated to be very thin (coating thickness is ~2 μm; see fig. S9), the thermal resistance is negligible (6.7×10^{-6} to 3.7×10^{-7} K W^{-1}). We also chose

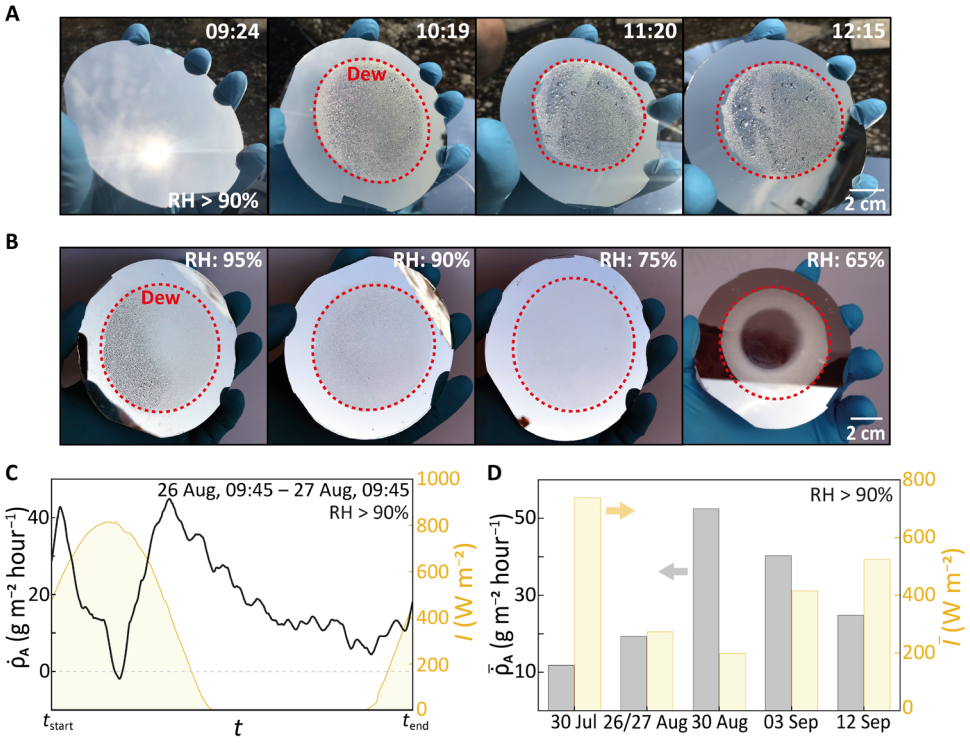


Fig. 3. Dew harvesting experiments. (**A**) Qualitative images of dew harvesting under direct solar radiation. (**B**) Dew formation under solar irradiation, 90 min after the emitter is exposed to various (95 to 65%) levels of constant RH. (**C**) Dew mass flux and solar irradiation over 24 hours at RH > 90%. (**D**) Mean dew mass flux and mean irradiation for five experimental runs, demonstrating broad operational capability. More information can be found in table S1. Photo credit: Tobias Gulich, ETH Zurich.

this coating due to its ease of fabrication, scalability, robust superhydrophobic performance, and low price compared to metallic coatings (*64*). The scanning electron microscope (SEM) image in Fig. 4A reveals the hierarchical nature of the condensation coating. Moreover, Fig. 4A shows a long-exposure photograph that unveils traces of the jumping droplets, illustrating the self-detaching mechanism of the droplets on our coating. The downward facing orientation avoids the risk of droplets rebounding onto the surface and lets them fall into a collection reservoir.

An indoor experimental chamber allows to study and quantify the passive harvesting mechanism. A Peltier element mimics outdoor experiments with the same dew mass fluxes (see Materials and Methods and fig. S10). Figure 4B shows the results, where the coating demonstrates a good repeatability for 1.5-hour runs ($N = 9$). For continuous operation, due to the inherently mild conditions of the process, the condensation coating is not expected to show deterioration even after longer exposure to a high humidity. During further 12-hour runs ($N = 2$), the coating yields the same mean dew mass flux (28.1 g m^{-2} hour^{-1}) as in the 1.5-hour experiments (28.6 g m^{-2} hour^{-1}), as depicted in Fig. 4C. The short period (<20 min) to reach steady-state flux is very advantageous, as the sample quickly yields water when environmental conditions are favorable. A comparison of the collected mass of dew below the condenser with and without our superhydrophobic CNF coating amply supports the necessity of the CNF coating for efficient and fully passive water removal (see fig. S11). To test the CNF coating under outdoor conditions, we mounted the selective emitter with the coating on the bottom side onto our experimental chamber and placed it at the same location as previously. For 39 hours (8 October 2020, 10:00 until 10 October 2020, 01:00), we exposed the CNF coating to the humid air (RH ≈ 90 to 95%) inside our chamber. The self-removed droplets were collected in a petri dish underneath the CNF coating. Moreover, our system also proves to work under real-world conditions, i.e., when the bottom of the selective emitter (CNF coating) operates in an open system. To evidence this, we created a Styrofoam box with a cut-through hole and mounted the selective emitter with radiation shield on top of it. During the experiment (14 October 2020, 17:00 until 15 October 2020, 11:00), the CNF coating was exposed to humid ambient air (mean RH: 83%), and the passively harvested water could fall into a petri dish underneath the CNF surface (for more details, see the Supplementary Materials and fig. S12). Last, an analysis of the harvested water indicates no contamination with Cr ions or CNF traces (see fig. S13).

DISCUSSION

We demonstrated a high-performance, fully passive, continuously operating atmospheric water harvesting system, working autonomously, without additional energy input requirement. The system concept exploits the synergistic effect of atmospheric radiative cooling and self-removed dropwise condensation of atmospheric water. The two mechanisms are optimized separately, each on one side of the same emitter-condenser sample, enabling 24-hour dew collection. A spectrally selective emitter enables minimal solar absorption during the day while maintaining a high emissivity outside the solar range, especially in the atmospheric transparency window (8 to 13 μm). Most importantly, based on a complete analysis of the involved heat fluxes and experimental constraints, an engineered

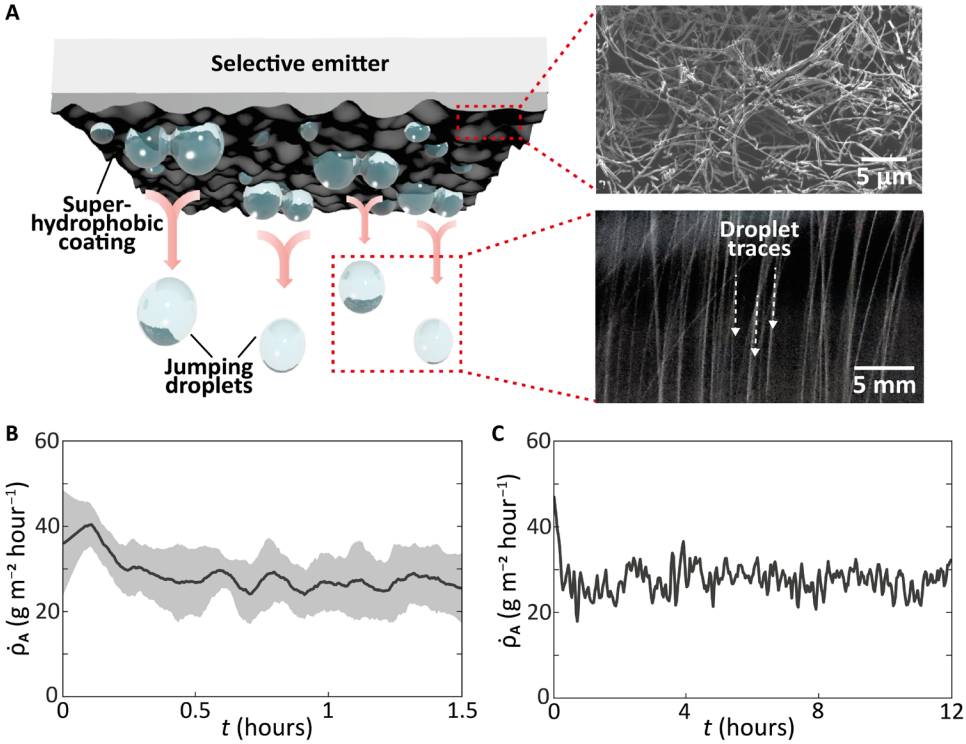


Fig. 4. Self-removal mechanism of CNF coating. (**A**) Working principle of superhydrophobic coating, promoting self-removal of droplets. Top right: SEM image of the CNF coating, verifying the hierarchical micro-/nanostructure. Bottom right: Long exposure image of coalescence-induced jumping, showing traces of detached droplets. (**B**) Dew mass flux rate of condensation coating (mean: 28.6 g m^{-2} hour^{-1}; $N = 9$). Gray area represents SD. (**C**) Twelve-hour durability test of CNF coating (mean: 28.1 g m^{-2} hour^{-1}; $N = 2$).

optimized radiation shield markedly enhances the dew harvesting performance through accounting for the surrounding radiative environment of the selective emitter. The shield minimizes absorption of atmospheric radiation and helps guide thermal radiation of the emitter toward low zenith angles, where the transparency of the atmosphere is highest. This results in at least doubling the yield of the state of the art and the pure selective emitter. Fully passive dew collection is facilitated through a superhydrophobic nanocomposite coating, which promotes dropwise condensation and self-removal of droplets through a coalescence-driven droplet jumping mechanism. The synergistic effect of the selective emitter, collaboratively working with the radiation shield, allows us to demonstrate dew harvesting at an RH as low as 65% under direct solar radiation and for a markedly larger dew harvesting period than the state of the art. Our system shows a dew harvesting capability close to the theoretical limit under even more demanding conditions, i.e., at a lower RH, during daytime and with convective heat gains (*30*). Further, we validated the real-world feasibility of our system in outdoor experiments, where we collect atmospheric water in a completely passive manner. Because of its entirely passive nature, continuity of operation, facility of use, and modularity, which allows it be complementary to a host of other water harvesting approaches (*65*, *66*), we expect our system to have a major impact toward our quest for high-performance, atmospheric water harvesting systems, overcoming impracticalities through the requirement of active user intervention. Last, while our work focused on the optimization of the radiation shield based on our experimental constraints, it opens up new ways for further work in maximizing the performance of any radiative cooling material through accounting for the surrounding radiative environment of the emitting surface (*62*).

MATERIALS AND METHODS

Fabrication of selective emitter

The fabrication of the selective emitter involves deposition of Ag and Cr on a JGS2 fused silica wafer with thermal evaporation (Evatec BAK501 LL). We spin-coated PDMS Sylgard 184 from Dow Corning on the other side of the same wafer, with a w/w mixing ratio of prepolymer:curing agent of 10:1. Parameters were 580 rpm, duration of 60 s, and 20 rps acceleration. After spin-coating, we cured the samples at 80°C for 1 hour. To characterize the optical properties of the selective emitter in the visible regime (0.25 to 2.5 μm), the UV/VIS NIR Spectrometer (V770) with an ILN-925 integrating sphere at normal incidence reveals the transmissivity and reflectivity values. We carried out IR characterization (2.5 to 20 μm) at near-normal incidence angle of 12° with a Fourier transform infrared (FTIR) spectrometer (Thermo Fisher Scientific) along with a gold-coated IR integrating sphere (Pike Technologies).

Mass data treatment

To quantify the dew mass flux, $\dot{\rho}_A$, a load cell type precision scale (G&G, JJ200B) with a resolution of 0.001 g measures the accumulated mass on the selective emitter. The rate of change of the accumulated dew with respect to time is $\dot{m} = \frac{dm}{dt}$. We derived the signal

from the scale with a Savitzky-Golay filter (*67*) and fixed the noise limit at 20 mg (versus scale resolution of 1 mg). The characteristic time is $f_c \approx 10$ min.

Fabrication and characterization of CNF coating

For the fabrication of the CNF coating, we closely follow the process in (*64*). CNFs (Sigma-Aldrich, 20 to 200 μm length, 100 nm diameter, 98% purity) and PTFE (Sigma-Aldrich, particle size 1 μm) are first dispersed in dichloromethane (CH_2Cl_2, Sigma-Aldrich) separately. We sonicate the CNF dichloromethane dispersion for 1 min with a probe ultrasonicator and the PTFE dichloromethane for 20 min with an ultrasonicator. Then, we mix the two dispersions and the mixture is further sonicated for 5 min with an ultrasonicator. The composite dispersion is then spray-coated on the required substrate (pressure of 4 bar). After that, we bake the coated sample at 400°C for 30 min in N_2 environment (*64*). After baking, the sample is cooled down at room temperature.

We performed SEM (Hitachi SU8230) to verify the hierarchical micro-/nanostructure of the coating (see Fig. 4A). We also measured the coating thickness after sectioning with a focused ion beam (FIB) and determined it to be about 2 μm, as shown in fig. S9. We determined the advancing contact angle, receding contact angle, and contact angle hysteresis of a water droplet on the PTFE-CNF coating using an optical contact angle measuring and contour analysis system (OCA 35 DataPhysics, Germany), with 8 μl of deionized water droplet for all the measurements. The advancing contact angle is 161.2° ± 0.8°, while the receding contact angle is 159.4° ± 0.9°, i.e., a contact angle hysteresis of ~2°.

Indoor experimental setup

For the indoor experiments, we rebuilt the same chamber as the one for outdoor experiments, but with an increased height for more accessibility. A Phidgets Hum1000_0 sensor records temperature/humidity inside the chamber, and a Peltier (Laird MS2-192-14-20-11-18), attached to a copper disk (0.5 mm thick, 4 inch diameter) with thermal paste, emulates the cooling power. To avoid any noise induced through mechanical stress, standard wires on the Peltier are replaced by fine-gauge wires. Peltier heat dissipation is guaranteed by a fan (Jamicon KF0510S1H-012-243R) running at a reduced voltage (2.3 V). A fan (FORCECON DFB803812MDOT) ensures fast and homogeneous diffusion of water vapor inside the chamber and is turned off before the start of the experiments to let the system operate fully passively. To start experiments, the Peltier receives a constant voltage (2.4 V) and a load cell type scale (G&G, JJ200B) measures dew mass accumulation. The Peltier cooling power and the RH inside the chamber are comparable to the outdoor experimental conditions of the run on 30 August 2019. Consequently, the mean dew mass flux $\bar{p}_A$ and the RH are at a comparable level, as shown in fig. S10.

Water quality analysis

We carried out conductivity measurements for ultrapure water (CHROMASOLV LC-MS Ultra tested for UHPLC-MS, Riedel-de Haën), tap water, and a 0.9 weight % (wt %) NaCl solution (dissolved in ultrapure water). We used two different tools (Greisinger GLF 100 Multi tester TDS and WTW LF 2000). Solutions were measured before and after being dripped over the CNF coating and recollected. We performed bright-field microscopy with an Olympus BX60 under ×10 magnification. The 0.03 wt % CNF in ultrapure water solution is sonicated immediately before imaging.

SUPPLEMENTARY MATERIALS

Supplementary material for this article is available at http://advances.sciencemag.org/cgi/content/full/7/26/eabf3978/DC1

REFERENCES AND NOTES

1. M. M. Mekonnen, A. Y. Hoekstra, Four billion people facing severe water scarcity. *Sci. Adv.* **2**, e1500323 (2016).
2. *Global Risks 2019, Insight Report* (World Economic Forum, ed. 14, 2019).
3. T. Gleeson, Y. Wada, M. F. P. Bierkens, L. P. H. van Beek, Water balance of global aquifers revealed by groundwater footprint. *Nature* **488**, 197–200 (2012).
4. B. K. Behera, P. K. Rout, S. Behera, *Move Towards Zero Hunger* (Springer, ed. 1, 2019).
5. R. E. Smalley, Future global energy prosperity: The terawatt challenge. *MRS Bull.* **30**, 412–417 (2005).
6. C. J. Vörösmarty, P. Green, J. Salisbury, R. B. Lammers, Global water resources: Vulnerability from climate change and population growth. *Science* **289**, 284–288 (2000).
7. P. H. Gleick, *Water in Crisis, A Guide to the World's Fresh Water Resources* (Oxford Univ. Press, 1993).
8. B. Khalil, J. Adamowski, A. Shabbir, C. Jang, M. Rojas, K. Reilly, B. Ozga-Zielinski, A review: Dew water collection from radiative passive collectors to recent developments of active collectors. *Sustain. Water Res. Manag.* **2**, 71–86 (2016).
9. B. Gido, E. Friedler, D. M. Broday, Liquid-desiccant vapor separation reduces the energy requirements of atmospheric moisture harvesting. *Environ. Sci. Technol.* **50**, 8362–8367 (2016).
10. D. Bergmair, S. J. Metz, H. C. de Lange, A. A. van Steenhoven, System analysis of membrane facilitated water generation from air humidity. *Desalination* **339**, 26–33 (2014).
11. R. V. Wahlgren, Atmospheric water vapour processor designs for potable water production: A review. *Water Res.* **35**, 1–22 (2001).
12. R. Li, Y. Shi, M. Wu, S. Hong, P. Wang, Improving atmospheric water production yield: Enabling multiple water harvesting cycles with nano sorbent. *Nano Energy* **67**, 104255 (2020).
13. N. Hanikel, M. S. Prévot, F. Fathieh, E. A. Kapustin, H. Lyu, H. Wang, N. J. Diercks, T. G. Glover, O. M. Yaghi, Rapid cycling and exceptional yield in a metal-organic framework water harvester. *ACS Central Sci.* **5**, 1699–1706 (2019).
14. X. Zhou, H. Lu, F. Zhao, G. Yu, Atmospheric water harvesting: A review of material and structural designs. *ACS Mater. Lett.* **2**, 671–684 (2020).
15. N. Hanikel, M. S. Prévot, O. M. Yaghi, MOF water harvesters. *Nat. Nanotechnol.* **15**, 348–355 (2020).
16. H. Jarimi, R. Powell, S. Riffat, Review of sustainable methods for atmospheric water harvesting. *Int. J. Low Carbon Technol.* **15**, 253–276 (2020).
17. H. Kim, S. Yang, S. R. Rao, S. Narayanan, E. A. Kapustin, H. Furukawa, A. S. Umans, O. M. Yaghi, E. N. Wang, Water harvesting from air with metal-organic frameworks powered by natural sunlight. *Science* **356**, 430–434 (2017).
18. F. Fathieh, M. J. Kalmutzki, E. A. Kapustin, P. J. Waller, J. Yang, O. M. Yaghi, Practical water production from desert air. *Sci. Adv.* **4**, eaat3198 (2018).
19. F. Zhao, X. Zhou, Y. Liu, Y. Shi, Y. Dai, G. Yu, Super moisture-absorbent gels for all-weather atmospheric water harvesting. *Adv. Mater.* **31**, e1806446 (2019).
20. W. E. Alnaser, A. Barakat, Use of condensed water vapour from the atmosphere for irrigation in Bahrain. *Appl. Energy* **65**, 3–18 (2000).
21. S. V. Boriskina, A. Raza, T. Zhang, P. Wang, L. Zhou, J. Zhu, Nanomaterials for the water-energy nexus. *MRS Bull.* **44**, 59–66 (2019).
22. S. M. Berkowicz, D. Beysens, I. Milimouk, M. Muselli, B. G. Heusinkveld, E. Wakshal, A. F. G. Jacobs, Urban dew collection under semi-arid conditions: Jerusalem, in *The Third International Conferene on Fog, Fog Collection and Dew, Pretoria, 11-15 October 2004*, D. Moller, ed. (University of Pretoria, South Africa, 2004).
23. D. Beysens, M. Muselli, I. Milimouk, C. Ohayon, S. Berkowicz, E. Soyeux, M. Mileta, P. Ortega, Application of passive radiative cooling for dew condensation. *Energy* **31**, 2303–2315 (2006).
24. T. Nilsson, W. E. Vargas, G. A. Niklasson, C. G. Granqvist, Condensation of water by radiative cooling. *Renew. Energy* **5**, 310–317 (1994).
25. O. Clus, P. Ortega, M. Muselli, I. Milimouk, D. Beysens, Study of dew water collection in humid tropical islands. *J. Hydrol.* **361**, 159–171 (2008).
26. M. Muselli, D. Beysens, M. Mileta, I. Milimouk, Dew and rain water collection in the Dalmatian Coast, Croatia. *Atmos. Res.* **92**, 455–463 (2009).
27. A. F. G. Jacobs, B. G. Heusinkveld, S. M. Berkowicz, Passive dew collection in a grassland area, The Netherlands. *Atmos. Res.* **87**, 377–385 (2008).
28. J. F. Maestre-Valero, R. Ragab, V. Martínez-Alvarez, A. Baille, Estimation of dew yield from radiative condensers by means of an energy balance model. *J. Hydrol.* **460–461**, 103–109 (2012).
29. I. Lekouch, K. Lekouch, M. Muselli, A. Mongruel, B. Kabbachi, D. Beysens, Rooftop dew, fog and rain collection in southwest Morocco and predictive dew modeling using neural networks. *J. Hydrol.* **448–449**, 60–72 (2012).

30. M. Dong, Z. Zhang, Y. Shi, X. Zhao, S. Fan, Z. Chen, Fundamental limits of the dew-harvesting technology. *Nanoscale Microscale Thermophys. Eng.* **24**, 43–52 (2020).
31. A. P. Raman, M. A. Anoma, L. Zhu, E. Rephaeli, S. Fan, Passive radiative cooling below ambient air temperature under direct sunlight. *Nature* **515**, 540–544 (2014).
32. J. Mandal, Y. Fu, A. C. Overvig, M. Jia, K. Sun, N. N. Shi, H. Zhou, X. Xiao, N. Yu, Y. Yang, Hierarchically porous polymer coatings for highly efficient passive daytime radiative cooling. *Science* **362**, 315–319 (2018).
33. Y. Zhai, Y. Ma, S. N. David, D. Zhao, R. Lou, G. Tan, R. Yang, X. Yin, Scalable-manufactured randomized glass-polymer hybrid metamaterial for daytime radiative cooling. *Science* **355**, 1062–1066 (2017).
34. Z. Chen, L. Zhu, A. Raman, S. Fan, Radiative cooling to deep sub-freezing temperatures through a 24-h day-night cycle. *Nat. Commun.* **7**, 13729 (2016).
35. M. Zhou, H. Song, X. Xu, A. Shahsafi, Z. Xia, Z. Ma, M. A. Kats, J. Zhu, B. S. Ooi, Q. Gan, Z. Yu, in *New Concepts in Solar and Thermal Radiation Conversion II*, J. N. Munday, P. Bermel, eds. (SPIE, 2019), p. 6.
36. L. Zhou, H. Song, J. Liang, M. Singer, M. Zhou, E. Stegenburgs, N. Zhang, C. Xu, T. Ng, Z. Yu, B. Ooi, Q. Gan, A polydimethylsiloxane-coated metal structure for all-day radiative cooling. *Nat. Sustain.* **2**, 718–724 (2019).
37. T. Li, Y. Zhai, S. He, W. Gan, Z. Wei, M. Heidarinejad, D. Dalgo, R. Mi, X. Zhao, J. Song, J. Dai, C. Chen, A. Aili, A. Vellore, A. Martini, R. Yang, J. Srebric, X. Yin, L. Hu, A radiative cooling structural material. *Science* **364**, 760–763 (2019).
38. A. R. Gentle, A. Nuhoglu, M. D. Arnold, G. B. Smith, in *Thermal Radiation Management for Energy Applications*, M. M. Al-Jassim, P. Bermel, eds. (SPIE, 2017), p. 10.
39. G. B. Smith, Amplified radiative cooling via optimised combinations of aperture geometry and spectral emittance profiles of surfaces and the atmosphere. *Solar Energ. Mater. Solar Cells* **93**, 1696–1701 (2009).
40. A. R. Gentle, G. B. Smith, Radiative heat pumping from the Earth using surface phonon resonant nanoparticles. *Nano Lett.* **10**, 373–379 (2010).
41. M. Muselli, D. Beysens, J. Marcillat, I. Milimouk, T. Nilsson, A. Louche, Dew water collector for potable water in Ajaccio (Corsica Island, France). *Atmos. Res.* **64**, 297–312 (2002).
42. E. M. Lushiku, A. Hjortsberg, C. G. Granqvist, Radiative cooling with selectively infrared-emitting ammonia gas. *J. Appl. Phys.* **53**, 5526–5530 (1982).
43. X. Yin, R. Yang, G. Tan, S. Fan, Terrestrial radiative cooling: Using the cold universe as a renewable and sustainable energy source. *Science* **370**, 786–791 (2020).
44. D. Li, X. Liu, W. Li, Z. Lin, B. Zhu, Z. Li, J. Li, B. Li, S. Fan, J. Xie, J. Zhu, Scalable and hierarchically designed polymer film as a selective thermal emitter for high-performance all-day radiative cooling. *Nat. Nanotechnol.* **16**, 153–158 (2021).
45. C. G. Granqvist, A. Hjortsberg, Radiative cooling to low temperatures: General considerations and application to selectively emitting SiO films. *J. Appl. Phys.* **52**, 4205–4220 (1981).
46. B. Bartoli, S. Catalanotti, B. Coluzzi, V. Cuomo, V. Silvestrini, G. Troise, Nocturnal and diurnal performances of selective radiators. *Appl. Energy* **3**, 267–286 (1977).
47. S. Catalanotti, V. Cuomo, G. Piro, D. Ruggi, V. Silvestrini, G. Troise, The radiative cooling of selective surfaces. *Solar Energ.* **17**, 83–89 (1975).
48. J. B. Boreyko, C.-H. Chen, Self-propelled dropwise condensate on superhydrophobic surfaces. *Phys. Rev. Lett.* **103**, 184501 (2009).
49. X. Chen, J. Wu, R. Ma, M. Hua, N. Koratkar, S. Yao, Z. Wang, Nanograssed micropyramidal architectures for continuous dropwise condensation. *Adv. Funct. Mater.* **21**, 4617–4623 (2011).
50. K. Rykaczewski, A. T. Paxson, S. Anand, X. Chen, Z. Wang, K. K. Varanasi, Multimode multidrop serial coalescence effects during condensation on hierarchical superhydrophobic surfaces. *Langmuir* **29**, 881–891 (2013).
51. Y. Cheng, B. Du, K. Wang, Y. Chen, Z. Lan, Z. Wang, X. Ma, Macrotextures-induced jumping relay of condensate droplets. *Appl. Phys. Lett.* **114**, 093704 (2019).
52. D. Wang, Q. Sun, M. J. Hokkanen, C. Zhang, F.-Y. Lin, Q. Liu, S.-P. Zhu, T. Zhou, Q. Chang, B. He, Q. Zhou, L. Chen, Z. Wang, R. H. A. Ras, X. Deng, Design of robust superhydrophobic surfaces. *Nature* **582**, 55–59 (2020).
53. A. Srinivasan, B. Czapla, J. Mayo, A. Narayanaswamy, Infrared dielectric function of polydimethylsiloxane and selective emission behavior. *Appl. Phys. Lett.* **109**, 061905 (2016).
54. M. Miler, Infrared absorption of glassy silicon dioxide. *Czechoslovak J. Phys.* **18**, 354–362 (1968).
55. J. Kou, Z. Jurado, Z. Chen, S. Fan, A. J. Minnich, Daytime radiative cooling using near-black infrared emitters. *ACS Photon.* **4**, 626–630 (2017).
56. A. Leroy, B. Bhatia, C. C. Kelsall, P. A. Castillejo-Cuberos, M. Di CapuaH, L. Zhao, L. Zhang, A. M. Guzman, E. N. Wang, High-performance subambient radiative cooling enabled by optically selective and thermally insulating polyethylene aerogel. *Sci. Adv.* **5**, eaat9480 (2019).
57. X. Wang, X. Liu, Z. Li, H. Zhang, Z. Yang, H. Zhou, T. Fan, Scalable flexible hybrid membranes with photonic structures for daytime radiative cooling. *Adv. Funct. Mater.* **30**, 1907562 (2020).
58. B. Czapla, A. Srinivasan, Q. Yin, A. Narayanaswamy, Potential for passive radiative cooling by PDMS selective emitters, in *Proceedings of the ASME 2017 Heat Transfer Summer Conference*, Bellevue, WA, 9 to 12 July 2017.
59. S. Y. Jeong, C. Y. Tso, Y. M. Wong, C. Chao, B. Huang, Daytime passive radiative cooling by ultra emissive bio-inspired polymeric surface. *Solar Energ. Mater. Solar Cells* , 110296 (2019).
60. E. A. Goldstein, A. P. Raman, S. Fan, Subambient nonevaporative fluid cooling with the sky. *Nat. Energy* **2**, 17143 (2017).
61. L. Li, B. Wang, R. Bader, J. Zapata, W. Lipiński, Reflective optics for redirecting convergent radiative beams in concentrating solar applications. *Solar Energ.* **191**, 707–718 (2019).
62. B. Bhatia, A. Leroy, Y. Shen, L. Zhao, M. Gianello, D. Li, T. Gu, J. Hu, M. Soljačić, E. N. Wang, Passive directional sub-ambient daytime radiative cooling. *Nat. Commun.* **9**, 5001 (2018).
63. D. K. Nandakumar, Y. Zhang, S. K. Ravi, N. Guo, C. Zhang, S. C. Tan, Solar energy triggered clean water harvesting from humid air existing above sea surface enabled by a hydrogel with ultrahigh hygroscopicity. *Adv. Mater.* **31**, e1806730 (2019).
64. M. Donati, C. W. E. Lam, A. Milionis, C. S. Sharma, A. Tripathy, A. Zendeli, D. Poulikakos, Sprayable thin and robust carbon nanofiber composite coating for extreme jumping dropwise condensation performance. *Adv. Mater. Interfaces* **8**, 2001176 (2021).
65. R. Li, Y. Shi, M. Alsaedi, M. Wu, L. Shi, P. Wang, Hybrid hydrogel with high water vapor harvesting capacity for deployable solar-driven atmospheric water generator. *Environ. Sci. Technol.* **52**, 11367–11377 (2018).
66. H. Kim, S. R. Rao, E. A. Kapustin, L. Zhao, S. Yang, O. M. Yaghi, E. N. Wang, Adsorption-based atmospheric water harvesting device for arid climates. *Nat. Commun.* **9**, 1191 (2018).
67. P. A. Gorry, General least-squares smoothing and differentiation by the convolution (Savitzky-Golay) method. *Anal. Chem.* **62**, 570–573 (1990).

Acknowledgments: We acknowledge the assistance of L. Steinmann, P. Feusi, and J. Vidic (all from ETH Zurich) for technical support; H. Albers for support with experiments; H. Lambley with imaging; R. Prasher (Lawrence Berkeley National Laboratory) for giving access to FTIR spectrometry; Swiss Meteo and IAC, ETH Zurich, for meteorological data; and Solar Topo (Obstalden, Switzerland) for providing solar zenith angle data. **Funding:** This work was financially supported by the Swiss National Science Foundation under grant number 179062 and by the European Union's Horizon 2020 research and innovation programme under grant number 801229 (HARMoNIC). **Author contributions:** T.M.S. and D.P. conceived the research idea and designed the study. T.M.S., G.S., and D.P. provided scientific guidance throughout. I.H. and G.S. designed the radiation side and implemented theory. I.H. fabricated samples and characterized the materials. I.H., T.G., and H.P. conducted experiments. I.H., H.P., T.G., G.S., and M.R. analyzed the data. A.M. designed and A.T. fabricated the superhydrophobic coating of the water condensation surface. I.H., T.M.S., G.S., H.P., and D.P. wrote the paper. All authors have read and approved the final version of the paper. **Competing interests:** The authors declare that they have no competing interests. **Data and materials availability:** All data needed to evaluate the conclusions in the paper are present in the paper and/or the Supplementary Materials. Figure source data can be found in the Eidgenössische Technische Hochschule Zürich Research Collection under https://research-collection.ethz.ch/handle/20.500.11850/469811.

Submitted 3 November 2020
Accepted 10 May 2021
Published 23 June 2021
10.1126/sciadv.abf3978

Citation: I. Haechler, H. Park, G. Schnoering, T. Gulich, M. Rohner, A. Tripathy, A. Milionis, T. M. Schutzius, D. Poulikakos, Exploiting radiative cooling for uninterrupted 24-hour water harvesting from the atmosphere. *Sci. Adv.* **7**, eabf3978 (2021).